Exploring the Impact of Systematic Bias in Type Ia Supernova Cosmology Across Diverse Dark Energy Parametrizations

Drishti Sharma [1,*] Purba Mukherjee [2,3,†] Anjan A Sen [2,‡] and Suhail Dhawan [4,§]

[1] Department of Physics, Jamia Millia Islamia, New Delhi-110025, India
[2] Centre for Theoretical Physics, Jamia Millia Islamia, New Delhi-110025, India
[3] Korea Astronomy and Space Science Institute, Daejeon 34055, Republic of Korea
[4] School of Physics & Astronomy and Institute of Gravitational Wave Astronomy, University of Birmingham, UK

We investigate the impact of instrumental and astrophysical systematics on dark energy constraints derived from Type Ia supernova (SN-Ia) observations. Using simulated datasets consistent with current SN-Ia measurements, we explore how uncertainties in photometric calibration, intergalactic dust, progenitor evolution in luminosity and light-curve stretch, and intrinsic color scatter affect the inferred dark energy equation of state parameters (w_0, w_a). We test the Generalised Scale Factor (GEN) evolution and benchmark it against three time-evolving dark energy models; namely Chevallier-Polarski-Linder (CPL), Jassal–Bagla–Padmanabhan (JBP) and Logarithmic (LOG) parametrizations; comparing their sensitivity to these systematic effects. Calibration biases and progenitor evolution emerge as the dominant sources of uncertainty, while simpler parametrisations, viz. GEN, which directly describes the expansion rate, remains relatively stable under all systematic injections, unlike CPL, JBP and LOG that rely on the dark energy equation of state. These findings underscore the need for sub-per cent calibration precision and enhanced astrophysical modelling to ensure the robustness of dark energy inferences from current and future SN-Ia cosmology experiments.

I. INTRODUCTION

Over the past few decades, cosmology has advanced dramatically, driven by high-precision measurements from the cosmic microwave background (CMB) [1–3], Type Ia supernovae (SN-Ia) [4, 5], baryon acoustic oscillations (BAO) and large-scale structure (LSS) [6–8] surveys. Together, these observations form the basis of the standard cosmological model, ΛCDM, which describes a spatially flat Universe composed primarily of cold dark matter (CDM) and dark energy (DE). Although the cosmological constant (Λ) serves as the simplest form of dark energy and successfully explains the observed late-time acceleration, its physical interpretation remains unresolved [9–11]. Hence, understanding the physical origin of this 'dark energy' is a fundamental question in modern cosmology.

The discovery of accelerated expansion of the Universe in late times, inferred from the luminosity–distance relation of SN-Ia, remains one of the most significant results in cosmology [12, 13]. Since then, SN-Ia have been established as a cornerstone of empirical dark energy studies, allowing measurements of the DE equation of state (EoS) parameter ($w = p_{\rm DE}/\rho_{\rm DE}$) [14–16]. The most widely used time-evolving dark energy model is the Chevallier-Polarski-Linder (CPL) [17, 18] parametrization, given by $w(a) = w_0 + w_a(1 - a)$, where w_0 denotes the present-day value of the EoS, w_a describes its evolution with the scale factor a. When combined with CMB anisotropies and BAO distance measurements, SN-Ia provide powerful constraints on w_0 and w_a, which for $w_0 = -1$ and $w_a = 0$ reduce to the concordance ΛCDM scenario [5, 19, 20]. Despite its successes, ΛCDM faces several challenges: local measurements of the Hubble constant differ from CMB-inferred values by $> 5\sigma$ [21], the amplitude of matter fluctuations exhibits a mild tension with predictions from the CMB [22–26]. Observations of unexpectedly massive galaxies by the James Webb Space Telescope (JWST) at high redshift also challenge the concordance framework [27, 28].

Recent high-precision galaxy redshift surveys, such as Dark Energy Spectroscopic Instrument (DESI), allow accurate measurements of the baryon acoustic oscillation scale over $0.1 < z < 3.5$ [29]. When combined with CMB and SN-Ia data, these observations hint at a time-varying dark energy component at the $\sim 2.8 - 4.2\sigma$ level [30] (depending on the SN-Ia sample and calibration method), motivating the exploration of dynamical dark energy beyond the canonical ΛCDM paradigm [31, 32]. Recent results by Mukherjee & Sen [33] identified seven characteristic redshifts, where the expansion history reconstructed using SN-Ia and BAO (anchored to Planck-2018 ΛCDM physics) shows $> 3\sigma$ deviations from Planck ΛCDM predictions for $z < 1$. As a follow-up, Choudhury, Mukherjee & Sen [34] examined the robustness of these characteristic redshifts and found them to remain stable under diverse DE parametrizations. Therefore, such discrepancies, if not for new physics beyond Λ, underscore the necessity of rigorously assessing systematic effects that can bias the cosmological parameter inference.

The reliability of supernova cosmology depends on accurate relative distance measurements across redshift. Redshift-dependent variations in supernova populations, calibration, or host-galaxy environments can introduce

* drishti2306519@st.jmi.ac.in
† pdf.pmukherjee@jmi.ac.in
‡ aasen@jmi.ac.in
§ s.dhawan@bham.ac.uk

biases that mimic or obscure true cosmological signals [35]. Low-redshift SN-Ia serve as the distance anchor for the Hubble diagram [5, 36, 37], but historically, they were observed with heterogeneous instruments, leading to significant calibration uncertainties [25, 38]. Modern wide-field surveys, such as the Zwicky Transient Facility (ZTF), now provide a uniformly observed and well-calibrated low-redshift sample, while contemporary high-redshift surveys offer greatly improved statistical precision [39–41]. The combination of these datasets is expected to enable a thorough assessment of systematic effects and their effect on DE measurements.

In this work, we investigate the impact of instrumental and astrophysical systematics on dark energy constraints derived from Type Ia supernovae, inspired by previous studies by Nordin *et al*[35] and Dhawan *et al*[42]. We consider a range of effects, including photometric calibration errors [38], intergalactic dust [43], progenitor evolution affecting luminosity [44] and light-curve stretch [45], as well as increased intrinsic scatter in color corrections [46]. Using simulated datasets consistent with current SN-Ia observations, we evaluate how these systematics influence the inferred dark energy parameters. We test the Generalised Scale Factor (GEN) [47, 48] evolution, analysing its susceptibility to the injected systematics, and compare the results with three time-evolving dark energy models, namely CPL, Jassal–Bagla–Padmanabhan (JBP) [49], Logarithmic (LOG) [50] parametrizations. By quantifying the sensitivity of (w_0, w_a) to each source of uncertainty, we identify which systematics are most likely to mimic the hints of evolving dark energy observed in recent combined SN-Ia, CMB, and DESI datasets, corresponding to deviations of $\sim 3\sigma$ from the concordance ΛCDM values of $w_0 = -1$ and $w_a = 0$ [30]. This analysis establishes benchmarks for understanding how unaccounted systematic effects can bias cosmological inference and highlights which dark energy models are more robust or least vulnerable to such uncertainties.

The paper is organised as follows. Section II presents the theoretical framework underlying dark energy models. Section III describes the observational datasets employed, including SN-Ia and complementary BAO and CMB measurements. Section IV details the methodology used to infer dark energy parameters. In Section V, we categorise the systematic effects studied, including calibration, intergalactic dust, progenitor evolution in luminosity and light-curve stretch, increased scatter in color corrections, and density parameter mismatches. Section VI presents the resulting impact of these systematics on the inferred dark energy constraints. Finally, Section VII summarises the main findings and discusses their implications for future surveys and the robustness of dark energy measurements.

II. THEORETICAL FRAMEWORK

We consider a spatially flat, homogeneous and isotropic Friedmann–Lemaître–Robertson–Walker (FLRW) universe. The expansion of the universe is described by the scale factor $a(t)$, with the Hubble parameter defined as

$$H(t) = \frac{\dot{a}(t)}{a(t)} . \tag{1}$$

The comoving distance D_M to a source at redshift z in the FLRW universe is

$$D_M(z) = \frac{c}{H_0} \int_0^z \frac{\mathrm{d}z'}{E(z')} , \tag{2}$$

where $E(z) \equiv H(z)/H_0$ is the normalised Hubble parameter, and the redshift is related to the scale factor by $1 + z = a_0/a$. Here, the subscript 0 indicates the present-day value of the corresponding quantity.

The expansion rate of the universe, described by $H(z)$, depends on the total energy density $\rho_{\mathrm{t}}(z)$ through Einstein's equations. This energy density is distributed among different components of the universe, primarily pressureless matter (baryons and cold dark matter) and dark energy with equation of state (EoS) $w_{\mathrm{DE}}(z) = p_{\mathrm{DE}}(z)/\rho_{\mathrm{DE}}(z)$. Consequently, $E(z)$ can be written as

$$E^2(z) = \Omega_{m0}(1+z)^3 + (1-\Omega_{m0}) \exp\left[3\int_0^z \frac{1+w(z')}{1+z'}\,\mathrm{d}z'\right] . \tag{3}$$

In this work, we consider a set of cosmological models to explore a broad range of systematic uncertainties in Type-Ia supernova cosmology, and their impact on the present-day equation of state w_0 and its evolution w_a. We test four representative cases:

1. Generalised Scale Factor (GEN) parametrization [47, 48]: Within the ΛCDM framework (neglecting radiation at late times), the scale factor has an exact solution,

$$a(t) = a_1 \left[\sinh\left(t/\tau\right)\right]^{2/3} , \tag{4}$$

where a_1 is an arbitrary dimensionless parameter and τ is a characteristic time scale, yielding

$$E^2(z) = \Omega_{m0}\,(1+z)^3 + 1 - \Omega_{m0} . \tag{5}$$

We consider a generalised extension of $a(t)$ to represent new physics, irrespective of any specific dark energy model,

$$a(t) = \tilde{a}_1 \left[\sinh\left(t/\tau\right)\right]^{B} , \tag{6}$$

which leads to

$$E^2(z) = A\,(1+z)^{2/B} + (1-A) , \tag{7}$$

with B a free parameter and $A = \frac{\tilde{a}_1^{2/B}}{\left(1+\tilde{a}_1^{2/B}\right)}$. The effective dark energy EoS is then

$$w(z) = \frac{w_T(z)\, E^2(z)}{E^2(z) - \Omega_{m0}\,(1+z)^3}\,, \tag{8}$$

where

$$w_T(z) = \frac{2A}{3B}\frac{(1+z)^{2/B}}{E^2(z)} - 1\,. \tag{9}$$

This allows us to directly evaluate $w_0 \equiv w(z=0)$ and $w_a \equiv \frac{\mathrm{d}w}{\mathrm{d}z}\big|_{z=0}$, where w_0 and w_a denote the present-day EoS and its linear variation, respectively.

2. Chevallier–Polarski–Linder (CPL) parametrization [17, 18]: The dark energy EoS is modelled as a first-order Taylor expansion in the scale factor a,

$$w(a) = w_0 + w_a\,(1-a)\,, \tag{10}$$

which in terms of redshift z becomes

$$w(z) = w_0 + w_a\,\frac{z}{1+z}\,. \tag{11}$$

3. Jassal–Bagla–Padmanabhan (JBP) parametrization [49]: The dark energy evolution peaks at intermediate redshifts and asymptotes to w_0 at both early and late times,

$$w(a) = w_0 + w_a\,(1-a)\,a\,, \tag{12}$$

which translates to

$$w(z) = w_0 + w_a\left(\frac{z}{1+z}\right)^2\,. \tag{13}$$

4. Logarithmic (LOG) parametrization [50]: This model describes a slowly varying DE EoS, expressed as

$$w(a) = w_0 - w_a\ln a\,, \tag{14}$$

or equivalently,

$$w(z) = w_0 + w_a\,\ln(1+z)\,. \tag{15}$$

Together, these four parametrizations allow us to test the robustness of cosmological constraints under different functional forms of $w(a)$.

III. OBSERVATIONAL DATA

We utilise the redshift distribution and noise covariance matrix from three key data sets:

- Pantheon-Plus SN-Ia: The Pantheon-Plus sample consists of $\sim$ 1500 spectroscopically-classified SN-Ia, spanning the redshift range $0.01 < z < 2.26$ [5]. It provides redshift-dependent measurements of the distance modulus $\mu(z)$,

$$\mu(z) = 5\log_{10}\left[\frac{D_L(z)}{1\,\mathrm{Mpc}}\right] + 25\,,\qquad D_L(z) = D_M\,(1+z)\,, \tag{16}$$

which connects the luminosity distance $D_L(z)$ of a source to its observed flux after accounting for the effects of cosmic expansion and redshift.

- DESI-DR2 BAO: We use 13 correlated baryon acoustic oscillation (BAO) distance measurements of D_M/r_d, D_H/r_d, and D_V/r_d from the DESI public data release 2, spanning the redshift range $0.1 < z < 4.2$ (see Table IV of [30]). Here

$$D_H(z) = \frac{c}{H(z)}\,, \tag{17}$$

is the Hubble distance, and

$$D_V(z) = \left[z\,D_M^2(z)\,D_H(z)\right]^{1/3}\,, \tag{18}$$

is the spherically averaged (isotropic) BAO distance. These are expressed in units of the comoving sound horizon at the drag epoch r_d. Assuming standard pre-recombination physics, r_d can be approximated as [51]

$$r_d \simeq 147.05\ \mathrm{Mpc}\ \times \left(\frac{\omega_b}{0.02236}\right)^{-0.13}\left(\frac{\omega_m}{0.1432}\right)^{-0.23}\left(\frac{N_{\rm eff}}{3.04}\right)^{-0.1}\,, \tag{19}$$

where $\omega_b = \Omega_b h^2$, $\omega_m = \Omega_{m0}h^2$ and $N_{\rm eff}$ is the effective no. of relativistic species.

- Compressed CMB: For the CMB, we adopt the compressed likelihood represented by a correlated Gaussian prior on the parameters $\{\theta_*, \omega_{bc}, \omega_b\}$. These are set by early-Universe physics and can be constrained independently of late-time effects, since contributions from the Integrated Sachs-Wolfe (ISW) effect and CMB lensing have been marginalised. The acoustic scale θ_* is defined as

$$\theta_* = \frac{r_s(z_*)}{D_A(z_*)}, \tag{20}$$

where $r_s(z_*)$ is the sound horizon at recombination and $D_A(z_*)$ the corresponding angular diameter distance. This compression is based on the `CamSpec` likelihood implementation, detailed in [52].

For SN-Ia, we generate mock distance moduli at the redshifts of Pantheon-Plus, propagating the quoted covariance matrix to incorporate both statistical and systematic uncertainties. For BAO, we simulate the distance measurements D_M/r_d, D_H/r_d, and D_V/r_d at the DESI tracer redshifts, adopting the reported covariance to model their correlations. For the CMB, we generate synthetic realisations of the compressed parameters $(\theta_*, \omega_b, \omega_m)$ drawn from a multivariate Gaussian comprising the mean vector and covariance matrix.

The mock data are constructed assuming a fiducial ΛCDM cosmology with $\Omega_{m0} = 0.3$, $H_0 = 70\ \mathrm{km\,s^{-1}\,Mpc^{-1}}$, $w_0 = -1$, and $w_a = 0$ for the CPL, JBP, and LOG parametrizations. For the GEN parametrization, we adopt $A = 0.3$ and $B = 2/3$. Injecting these fiducial values into the simulated observables allows us to isolate and test the impact of residual systematic effects in SN-Ia data.

IV. METHODOLOGY

The observed distance modulus for a Type Ia supernova is obtained from its peak apparent magnitude (m_B), light-curve stretch (x_1), and colour (c) as [53, 54]

$$\mu_{\mathrm{obs}} = m_B - (M_B - \alpha x_1 + \beta c) + \Delta M + \Delta B, \qquad (21)$$

where M_B is the absolute magnitude for a fiducial supernova with $x_1 = c = 0$. The parameters α and β describe the width–luminosity and colour–luminosity relations, while ΔM and ΔB account for host-galaxy luminosity and distance biases [46, 55].

In this work, we simulate mock realisations resembling the Pantheon-Plus SN-Ia sample, DESI BAO measurements, and the compressed CMB observables (see Section III) rather than using the real data directly. Cosmological parameter inference uses the full SN-Ia covariance matrix,

$$\mathcal{C}_{\mathrm{SN}} = \mathcal{C}_{\mathrm{stat}} + \mathcal{C}_{\mathrm{sys}}, \qquad (22)$$

with a Gaussian likelihood,

$$\chi^2_{\mathrm{SN}} = \Delta^T_{\mathrm{SN}} \cdot \mathcal{C}^{-1}_{\mathrm{SN}} \cdot \Delta_{\mathrm{SN}}\,, \qquad (23)$$

where,

$$\Delta_{\mathrm{SN}} = \mu_{\mathrm{mock}}(z) - \mu_{\mathrm{model}}(z)\,. \qquad (24)$$

For BAO, the likelihood is constructed from the measured distance ratios D_x/r_d (with $X \equiv M,\ H,\ V$) and their covariance $\mathcal{C}_{\mathrm{BAO}}$:

$$\chi^2_{\mathrm{BAO}} = \Delta^T_{\mathrm{BAO}} \cdot \mathcal{C}^{-1}_{\mathrm{BAO}} \cdot \Delta_{\mathrm{BAO}}\,, \qquad (25)$$

where,

$$\Delta_{\mathrm{BAO}} = \left[\frac{D_{X,\,\mathrm{mock}}}{r_d} - \frac{D_{X,\,\mathrm{model}}}{r_d}\right]. \qquad (26)$$

For the compressed CMB parameters $\{\theta_*, \omega_b, \omega_{bc}\}$, the Gaussian likelihood is defined using the computed mock mean vector $\boldsymbol{\mu}_{\mathrm{CMB}}$ and predicted covariance matrix $\mathcal{C}_{\mathrm{CMB}}$:

$$\chi^2_{\mathrm{CMB}} = \Delta^T_{\mathrm{CMB}} \cdot \mathcal{C}^{-1}_{\mathrm{CMB}} \cdot \Delta_{\mathrm{CMB}}\,, \qquad (27)$$

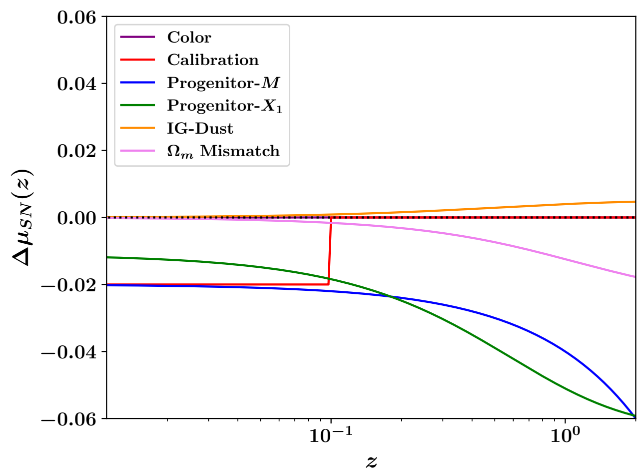

FIG. 1: Impact of injected SNIa systematic uncertainties on the Hubble residuals, illustrating how each source of systematics alters the inferred cosmological distances.

where,

$$\Delta_{\mathrm{CMB}} = \{\theta_*, \omega_b, \omega_m\}_{\mathrm{mock}} - \{\theta_*, \omega_b, \omega_m\}_{\mathrm{model}}\,. \qquad (28)$$

Assuming the datasets are independent, the combined likelihood is the sum of the individual χ^2 contributions:

$$\chi^2_{\mathrm{tot}} = \chi^2_{\mathrm{SN}} + \chi^2_{\mathrm{BAO}} + \chi^2_{\mathrm{CMB}}. \qquad (29)$$

This unified formalism allows simultaneous parameter inference from supernovae, in combination with BAO and CMB observables, while propagating correlations within each dataset.

We perform parameter sampling using the `emcee`[56] [57] MCMC ensemble sampler, evaluating the likelihood at each step within a Bayesian framework. Uniform (flat) priors are adopted on all model parameters, with ranges specified in Table I. The resulting posterior chains are analysed with `GetDist`[58] [59], which provides marginalized parameter constraints, contour plots, and statistical summaries.

TABLE I: Uniform (flat) priors adopted for cosmological parameters in our analysis. The dimensionless Hubble constant is defined as $h = H_0/(100\ \mathrm{km\,s^{-1}\,Mpc^{-1}})$.

Parameter	Prior range
h	$\mathcal{U}\,[0.3,\ 1.2]$
Ω_{m0}	$\mathcal{U}\,[0,\ 1]$
w_0	$\mathcal{U}\,[-3,\ 1]$
w_a	$\mathcal{U}\,[-3,\ 2]$
A	$\mathcal{U}\,[0,\ 1]$
B	$\mathcal{U}\,[0.4,\ 0.8]$

Note. All priors are uniform (flat) within the specified ranges. The chosen intervals are sufficiently broad to avoid constraining the posterior artificially while excluding unphysical values.

V. SYSTEMATIC GROUPINGS

Type Ia supernova cosmology is sensitive to a variety of systematic effects that can bias the inferred luminosity distances and, consequently, the constraints on dark energy. We classify these effects into broad categories, each motivated by astrophysical or observational considerations. In this section, we outline the physical origin of each source of systematics and the parametrizations we adopt to model their possible redshift dependence.

A. Calibration

A persistent challenge in SN-Ia cosmology arises from photometric calibration. Because low- and high-redshift SN-Ia are generally observed with different instruments, cross-calibration is required to bring them onto a common flux scale [5, 60]. The low-redshift anchor sample itself is heterogeneous, having been assembled from multiple telescopes and filter systems, many of which are no longer operational. Recent surveys such as Foundation [61], Zwicky Transient Facility (ZTF) [40], and Joint Light-curve Analysis(JLA) + Hubble Space Telescope (HST)/Vera C. Rubin Observatory Legacy Survey of Space and Time (LSST)-pathfinders [41] have sought to provide more uniform low-redshift datasets. Nonetheless, residual offsets between low- and high-redshift subsets remain possible.

To capture this effect, we model the calibration systematic as a step function in the B-band absolute magnitude:

$$M_B(z) = \begin{cases} M_B(0)\,, & z \leq 0.1 \\ M_B(0) + \Delta M_B\,, & z > 0.1 \end{cases} \tag{30}$$

where ΔM_B represents the magnitude offset between low- and high-redshift SN-Ia. In our analysis, we adopt an offset of $\Delta M_B = 0.02$ mag. This formulation allows us to quantify the impact of this constant calibration offset on the inferred dark energy parameters. The resulting parameter shifts in the w_0–w_a plane for all models are given in Table II.

B. Intergalactic Dust

While host-galaxy dust is routinely corrected for in SN-Ia light-curve analyses, either through empirical colour terms or extinction in the V band, absorption by intergalactic dust is typically neglected. Current constraints suggest that such a component represents only a tiny fraction of the total baryonic mass [43]. Nevertheless, even a low-density diffuse dust population could attenuate SN fluxes in a redshift-dependent manner, thereby biasing the distance–redshift relation and potentially mimicking cosmological effects. In particular, intergalactic dust could shift the inferred dark energy parameters.

Following [43], we describe the intergalactic dust density as a power-law function of redshift,

$$\rho_{\rm dust}(z) = \rho_{\rm dust,0}\,(1+z)^{\gamma}\,, \tag{31}$$

and scale it relative to the critical density $\rho_{c,0} = \frac{3H_0^2}{8\pi G}$ as

$$\rho_{\rm dust}(z) = \rho_{c,0}\,\Omega_{\rm dust}(1+z)^{\gamma}\,. \tag{32}$$

For our fiducial test, we adopt $\Omega_{\rm dust} = 5\times10^{-6}$ and $\gamma = -1$, corresponding to a very low-density dust component that decreases slowly with redshift.

Assuming the dust is spatially homogeneous but evolves with cosmic time—consistent with detections of diffuse dust several Mpc from galaxies [62]—the optical depth along the line of sight to a source at redshift z_s is given by

$$\tau_\lambda = \int_0^{z_s} \kappa_\lambda\,\rho_{\rm dust}(z)\,c\,\frac{{\rm d}t}{{\rm d}z}\,{\rm d}z\,. \tag{33}$$

Substituting our parametrization yields,

$$\tau_\lambda = \rho_{c,0}\,\Omega_{\rm dust}\int_0^{z_s} \kappa_\lambda\,\frac{(1+z_s)}{(1+z)}\,R_V(1+z)^{\gamma-1}\,\frac{{\rm d}z}{E(z)}\,. \tag{34}$$

Here, κ_λ denotes the wavelength-dependent mass absorption coefficient, for which we adopt $\kappa_V \simeq 1.5\times10^4\,{\rm cm^2\,g^{-1}}$ [63]. The corresponding shift in observed supernova magnitudes (Hubble residuals) is then given by

$$\Delta_{\rm HR} = -2.5\,\log_{10}\!\left(e^{-\tau_\lambda}\right) \simeq 1.086\,\tau_\lambda\,. \tag{35}$$

The induced shifts in the w_0–w_a parameter space due to intergalactic dust are summarised in Table II.

C. Progenitor Evolution in Luminosity

Spectroscopic studies of Type Ia supernovae at intermediate redshifts ($z \sim 0.5$) and at higher redshifts ($z > 1$) show that their optical properties remain largely consistent across cosmic time [44, 64, 65], with only modest deviations detected in the ultraviolet [66–68] limit. This generic similarity suggests that strong evolutionary effects in SN-Ia spectra are unlikely. However, a mild redshift-dependent drift in their intrinsic luminosity cannot be fully ruled out

To test for such an effect, we introduce a simple phenomenological model in which the absolute B-band magnitude evolves with redshift, as

$$M_B(z) = M_B(0) + \epsilon\,(1+z_{\rm CMB}), \tag{36}$$

where ϵ quantifies the slope of the luminosity evolution.

For our analysis, we adopt $\epsilon = 0.02$ mag, modest yet potentially significant luminosity evolution. This framework allows us to assess whether gradual changes in progenitor properties, such as metallicity or stellar age, producing a mild redshift-dependent shift in intrinsic SN-Ia brightness, could lead to systematic biases in the inferred cosmological parameters. See Table II for the resulting parameter shifts.

D. Progenitor Evolution in Light-Curve Stretch

The observable properties of Type Ia supernovae depend on progenitor characteristics, such as metallicity [69, 70] and stellar population age [71], which evolve with redshift. These changes can influence both intrinsic luminosity and light-curve shapes, particularly the stretch parameter x_1. Recent studies indicate that the width–luminosity correction may differ between low-x_1 and high-x_1 populations [45], implying that a redshift-dependent x_1 distribution could bias cosmological inferences if neglected.

We model this effect using a broken power-law for the stretch–luminosity coefficient α:

$$\alpha(x_1) = \begin{cases} \alpha_{\text{low}} &= 0.23\,, \quad x_1 < -0.49\,, \\ \alpha_{\text{high}} &= 0.13\,, \quad x_1 \geq -0.49\,. \end{cases}$$

This approach approximates the situation in which selection effects have been corrected, and the remaining offset between true and inferred distances arises from applying a single x_1-independent α to a population whose x_1 distribution evolves with redshift.

To model the redshift evolution of x_1, we follow the prescription of [72], which links the shift in x_1 to the local specific star-formation rate. We write the Hubble residual shift as

$$\Delta_{\text{HR}} = \alpha(x_1)\,\Delta x_1\,, \tag{37}$$

where $\alpha(x_1)$ is the stretch–luminosity slope and Δx_1 describes the redshift evolution of the stretch parameter. We parameterize Δx_1 as

$$\Delta x_1 = A\,\mu_1 + (1 - A)\left[a\,\mu_1 + (1 - a)\,\mu_2\right]\,, \tag{38}$$

with $a = 0.47$, $\mu_1 = 0.38$, and $\mu_2 = -1.26$, representing the conservative case from [72]. The factor A evolves with redshift as

$$A = K^{-1}(1 + z)^{2.8} + 1^{-1}\,, \tag{39}$$

which captures the population drift similar to the evolution predicted by [71]. While alternative parameter choices may modify the detailed evolution, this prescription provides a realistic baseline for testing the influence of progenitor evolution on the w_0–w_a constraints (see Table II). This framework allows us to quantify the bias introduced into the cosmological parameters if the evolving x_1 distribution is not fully accounted for.

E. Increased Scatter in Colour Correction

While systematic offsets primarily shift the relative distance modulus between low- and high-z SNe Ia, additional scatter increases the uncertainties without altering the mean. We model this effect by introducing extra dispersion in the colour–luminosity correction term (βc in the Tripp relation in Eq. (21)), represented as a systematic $\sigma(\beta)$. This captures potential variations in either the dust law slope or the intrinsic colour–luminosity relation.

In practice, the effect is implemented by inflating the covariance matrix. Specifically, we add a diagonal component corresponding to a constant error of $\sigma(\beta) \equiv \sigma_\beta = 0.15$ mag [5, 61], such that

$$\mathcal{C}' = \mathcal{C} + \sigma_\beta^2\,\mathrm{I}, \tag{40}$$

TABLE II: Parameter shifts and output slopes for various systematics and dark energy models.

Calibration Offset: $\Delta M_B = 0.02$				
Parameter Shift	**CPL**	**JBP**	**LOG**	**GEN**
ΔA	—	—	—	-0.0181
ΔB	—	—	—	-0.0100
Δw_0	-0.0763	-0.1208	-0.0622	-0.0197
Δw_a	$+0.1905$	$+0.5988$	$+0.1034$	-0.0411
Intergalactic Dust Modeling: $\Omega_{\text{dust}} = 5 \times 10^{-6}$				
Parameter Shift	**CPL**	**JBP**	**LOG**	**GEN**
ΔA	—	—	—	$+0.0002$
ΔB	—	—	—	-6.8×10^{-5}
Δw_0	$+0.0125$	$+0.0123$	$+0.0049$	$+0.0003$
Δw_a	-0.0333	-0.0532	-0.0021	$+0.0015$
Progenitor Evolution in M_B**:** $\epsilon = 0.02$				
Parameter Shift	**CPL**	**JBP**	**LOG**	**GEN**
ΔA	—	—	—	$+0.0135$
ΔB	—	—	—	$+0.0064$
Δw_0	$+0.0331$	$+0.0311$	$+0.0262$	$+0.0171$
Δw_a	-0.0676	-0.1064	-0.0310	$+0.0349$
Progenitor Evolution in x_1				
Parameter Shift	**CPL**	**JBP**	**LOG**	**GEN**
ΔA	—	—	—	$+0.0348$
ΔB	—	—	—	$+0.0168$
Δw_0	-0.0777	-0.1019	-0.0698	$+0.0391$
Δw_a	$+0.1562$	$+0.4140$	$+0.0947$	$+0.0756$
Color Correction: $\sigma_\beta = 0.15$				
Parameter Shift	**CPL**	**JBP**	**LOG**	**GEN**
ΔA	—	—	—	-1.2×10^{-4}
ΔB	—	—	—	-3.4×10^{-5}
Δw_0	$+0.0115$	$+0.0097$	$+0.0088$	-0.0001
Δw_a	-0.0387	-0.0509	-0.0159	-0.0003
Density Parameter Mismatch: $\Delta\Omega_m = 0.01$				
Parameter Shift	**CPL**	**JBP**	**LOG**	**GEN**
ΔA	—	—	—	—
ΔB	—	—	—	—
Δw_0	$+0.0257$	$+0.0319$	$+0.0177$	$+0.0123$
Δw_a	-0.0572	-0.1381	-0.0203	$+0.0247$

where $\mathcal{C}$ is the original covariance matrix and I is the identity matrix of dimension equal to the number of supernovae. The updated covariance $\mathcal{C}'$ is then utilised in the likelihood analysis. Although motivated here as colour-correction scatter, this framework can equally represent other forms of residual dispersion in the distance modulus. The impact on the w_0–w_a constraints for all models is summarized in Table II

F. Density Parameter Mismatch

Current constraints on the dark energy parameters rely on a joint analysis of early- and late-universe probes, namely the CMB, BAO, and SNIa. Within a flat ΛCDM framework, $(\Omega_{k0},\, w_0,\, w_a) = (0,\, -1,\, 0)$, a mild but notable tension arises: the matter density inferred from Planck $\Omega_{m0} = 0.315 \pm 0.007$ is lower than that inferred from DES SN-Ia $\Omega_{m0} = 0.357 \pm 0.017$, a discrepancy at the $\sim 2.5\sigma$ level.

Because Ω_{m0} is degenerate with w_0 and w_a in combined CMB+BAO+SN analyses, such a mismatch can shift the inferred confidence contours compared to the case where both early- and late-universe probes favour the same Ω_{m0}. To mimic this effect, we simulate a deliberate offset between the Ω_{m0} used to generate the SN-Ia Hubble diagram and the value adopted for the external datasets. A recent study by [73] explored how underlying dynamical dark energy cosmologies can induce biases in Ω_{m0} and H_0 when individual probes are analyzed under ΛCDM. In contrast to their work, our analysis examines the impact of such systematic offsets within the SN-Ia Hubble diagram and evaluates their propagation to the inferred (w_0, w_a) parameters across multiple dark energy parametrizations. While the physical origin of such a discrepancy could stem from unresolved systematics in any of the previously discussed categories, here we encapsulate it simply as an Ω_{m0} mismatch. This treatment serves as a proxy for an *unknown unknowns* - an effect that perturbs the observed μ-z relation but lacks a straightforward parametric form.

For the CPL, JBP, and LOG parametrizations, this effect is implemented directly as an offset in Ω_{m0}. In contrast, for the GEN parametrization, which is formulated in terms of the parameters A and B, the same mismatch is accounted for when transferring from $\{A, B\}$ to $\{w_0, w_a\}$, where Ω_{m0} enters implicitly through Eqs. (7) and (8). This allows the resulting (w_0, w_a) shifts to reflect the corresponding density mismatch within the GEN framework.

VI. IMPACT ON DARK ENERGY

The influence of the six systematic effects described in Section V is quantified in terms of their induced shifts in the inferred dark energy EoS parameters w_0 and w_a. The resulting Hubble residuals from these systematics injections, assuming the CPL model, are compared with the fiducial case in Figure 1 for illustration.

Table II summarises the parameter displacements for the four dark energy models considered, viz. CPL, JBP, LOG, and GEN, while Figures 2, 3 and 4 illustrate their direction and magnitude in the w_0–w_a plane for the four parametrizations studied here.

A. Effect of Individual Systematics

The six systematic scenarios lead to distinct patterns of parameter displacement, reflecting their physical origins and the structure of parameter degeneracies. Across most cases, the induced displacements align with the existing w_0–w_a degeneracy direction, indicating that systematics primarily bias the inferred evolution of dark energy rather than its overall normalisation.

1. A uniform magnitude bias of $\Delta M_B = 0.02$ produces one of the most pronounced effects across all models. The shift is maximum for the JBP parametrization with $\Delta w_0 \simeq -0.12$ and $\Delta w_a \simeq +0.60$, whereas it remains mild for GEN ($\Delta w_0 \simeq -0.02$, $\Delta w_a \simeq -0.04$). This behaviour reflects the strong sensitivity of luminosity distances to global calibration, which directly impacts the absolute brightness scale of the SN-Ia sample.

2. For a fiducial intergalactic dust density of $\Omega_{\rm dust} = 5 \times 10^{-6}$, the resulting shifts are minimal ($|\Delta w_0| < 0.02$, $|\Delta w_a| < 0.05$) for all models. Since the effect mainly rescales the overall flux level without introducing significant redshift dependence, it does not mimic late-time dark energy evolution. This confirms that intergalactic dust is unlikely to bias late-time dark energy inference at the level of current observational precision.

3. A mild intrinsic luminosity evolution, parametrized by $\epsilon = 0.02$, causes modest but coherent shifts in the w_0–w_a plane. Typical values are $\Delta w_0 \sim +0.03$ and $\Delta w_a \sim -0.07$ for CPL, with slightly smaller amplitudes for GEN. Although small in magnitude, this effect introduces a redshift-dependent bias that can imitate dark energy evolution, particularly in more flexible models like JBP.

4. Evolution in the stretch distribution, linked to host properties and star-formation rate, has a more significant impact than compared to progenitor evolution in M_B. It drives parameter displacements up to $\Delta w_0 \sim -0.08$ and $\Delta w_a \sim +0.40$ for the JBP model, again oriented along the degeneracy axis. Among progenitor-related sources, this mechanism contributes the largest bias, highlighting the need to model population drift in SN standardization.

5. Uncertainty in the colour–luminosity coefficient ($\sigma_\beta = 0.15$) broadens the error contours but yields negligible mean displacement ($|\Delta w_0| < 0.02$, $|\Delta w_a| < 0.05$).

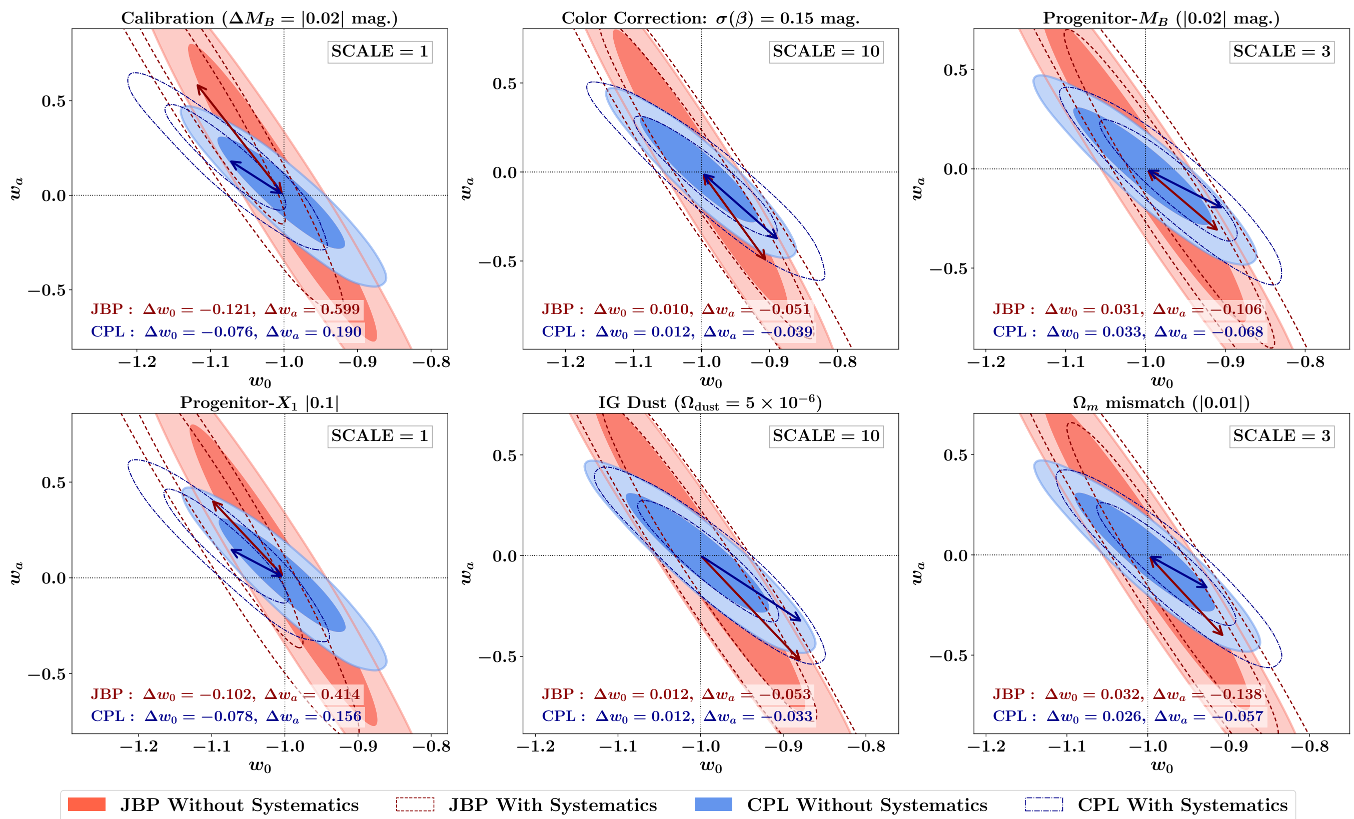

FIG. 2: Impact of injected Type Ia supernova systematics on cosmological parameter constraints from the CPL vs JBP models. Each panel shows the shift in the w_0–w_a plane resulting from a specific injected systematic (e.g., calibration, color correction, progenitor effects (on M and x_1), intergalactic dust, and Ω_m mismatch). Filled contours correspond to fits without systematics, while dashed contours indicate results after applying the injected systematic, scaled for better visualisation.

Its effect is statistically similar to increased photometric noise, primarily enlarging parameter uncertainties rather than significantly shifting the central estimates.

6. A shift of $\Delta\Omega_m = 0.01$ between the true and assumed cosmology induces small but coherent offsets in w_0 and w_a, with typical changes of $\Delta w_0 \simeq +0.03$ and $\Delta w_a \simeq -0.06$ for CPL. This reflects the degeneracy between the matter and dark energy densities at late times. The displacement remains subdominant compared to calibration or progenitor-related effects but traces a similar direction in parameter space.

Overall, in our analysis, calibration and progenitor evolution are found to be the main drivers of systematic bias in dark energy estimation from SNIa cosmology, while colour scatter and matter density mismatches play only minor roles, and intergalactic dust has a negligible effect. Across all cases studied, the directionality of the parameter shifts generally follows the w_0–w_a degeneracy, suggesting that most systematics primarily distort the inferred $w(z)$. The intergalactic dust effect induces a unidirectional shift, whereas the other systematics produce displacements on both sides of the degeneracy axis, depending on the sign and magnitude of the injection.

B. Comparative Analysis of DE Models

The impact of systematics is not uniform across different dark energy parametrizations. The intrinsic flexibility and degeneracy structure of each model determine how it responds to observational biases, influencing both the amplitude and direction of shifts in the w_0–w_a plane. A comparative analysis with respect to the commonly used CPL reveals clear trends in model sensitivity and stability:

1. The JBP model exhibits the largest systematic-induced displacements, particularly under calibration of M_B and progenitor-x_1 evolution. Its quadratic dependence on $z/(1+z)$ makes JBP more sensitive to redshift-dependent variations in luminosity, amplifying small biases into stronger shifts in the w_0–w_a plane compared to the linear CPL form.

2. The LOG parametrization closely mirrors the CPL scenario in both direction and magnitude of systematic

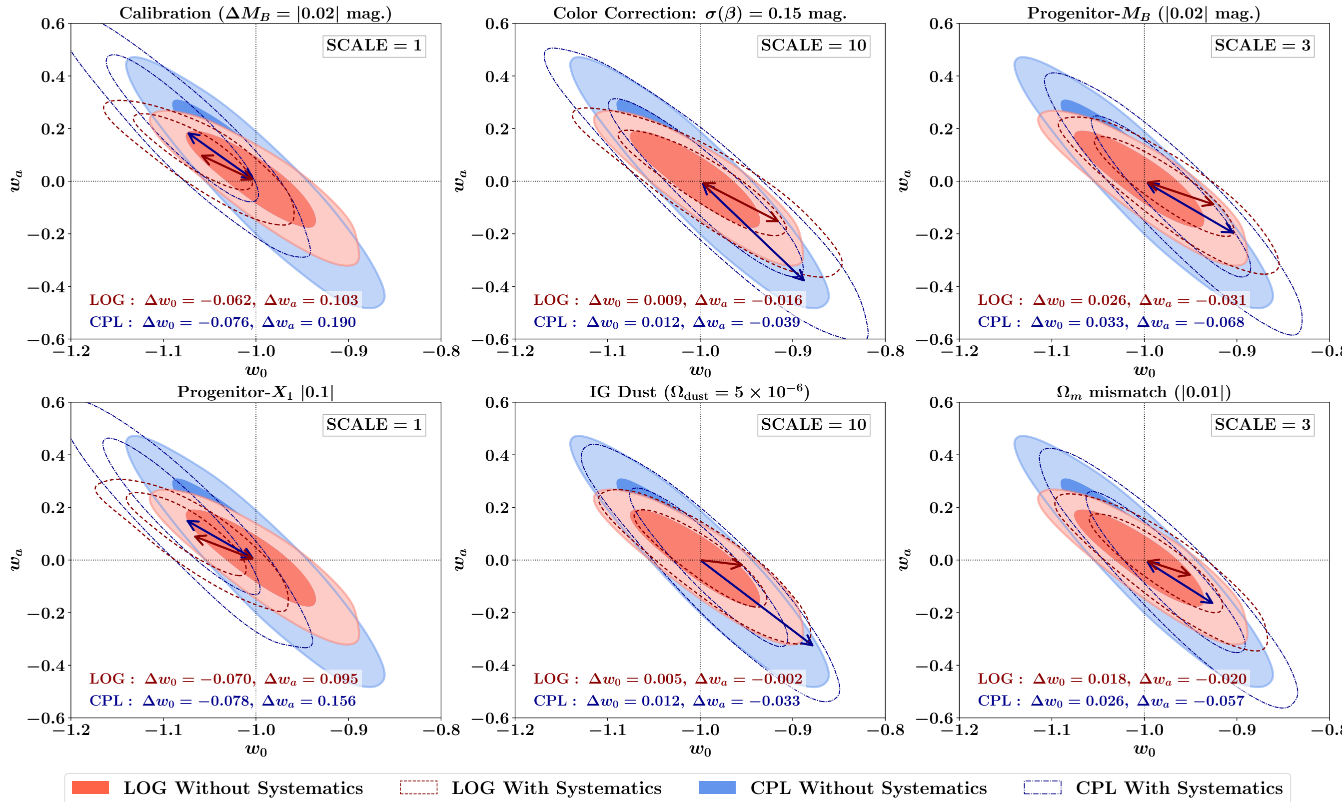

FIG. 3: Impact of injected SNIa systematics on the w_0–w_a constraints for the CPL vs LOG parametrizations. Panels illustrate how individual systematics shift the recovered contours. Filled contours denote fits without systematics; dashed contours show results after systematic injection.

shifts. Deviations arise only marginally, mainly for intergalactic dust, suggesting that a logarithmic evolution in $w(z)$ does not provide significant improvement in robustness over the linear CPL form.

3. The GEN model shows the least sensitivity to all systematic effects, particularly those arising from calibration and progenitor evolution. Its simpler functional form reduces sensitivity to redshift-dependent biases, making it the most robust among the tested models. This arises because, unlike CPL, JBP, and LOG, which directly parametrize $w(z)$, the GEN model parametrizes the expansion rate $E(z)$ (or equivalently, the energy density). Since $E(z)$ connects to distance measures through a single integration, whereas $w(z)$ affects them through a double integral, it appears that the GEN model is less affected by cumulative biases in the observed SNIa data.

Overall, these comparisons establish a clear trend in how SN-Ia systematics affect dark energy inference: JBP is the most affected, CPL and LOG show intermediate sensitivity, while GEN remains the least affected. This hierarchy demonstrates that the choice of the model or parametrization governs how strongly the inferred values of dark energy EoS parameters, w_0 and w_a, are susceptible to biases from supernova systematics. Since current SNIa data mainly probe $z \lesssim 1$, model selection plays a critical role in interpreting these constraints reliably.

For completeness, we further demonstrate the impact of various systematic uncertainties on the reconstructed cosmological quantities—the normalised Hubble parameter $E(z)$ (left panels), the distance modulus $\mu(z)$ (middle panels), and the dark energy equation of state $w(z)$ (right panels) in Fig. 5. The upper panels correspond to the CPL model, while the lower panels show the results for the GEN parameterisation. Each curve represents a different source of systematic effect, including calibration offset, color correction, progenitor mass and metallicity evolution, intergalactic dust, and matter density mismatch, compared to the fiducial (dotted black) cosmology. We find that all sources of systematics induce redshift-dependent deviations in the reconstructed quantities, with the calibration and progenitor effects producing the largest biases at low redshifts.

For the CPL case, the deviations in $E(z)$ and $\Delta\mu(z)$ rise rapidly at low $z < 1$, reaching a maximum around $z \approx 0.5$, and gradually decline towards higher $z > 1$. The corresponding impact on the reconstructed DE EoS $w(z)$ manifests as a smooth phantom-to-non-phantom transition, effectively mimicking a mild apparent evolution of $w(z)$ with redshift. In contrast, for the GEN parametrisation, the deviations in $E(z)$ and $\Delta\mu(z)$ begin to emerge

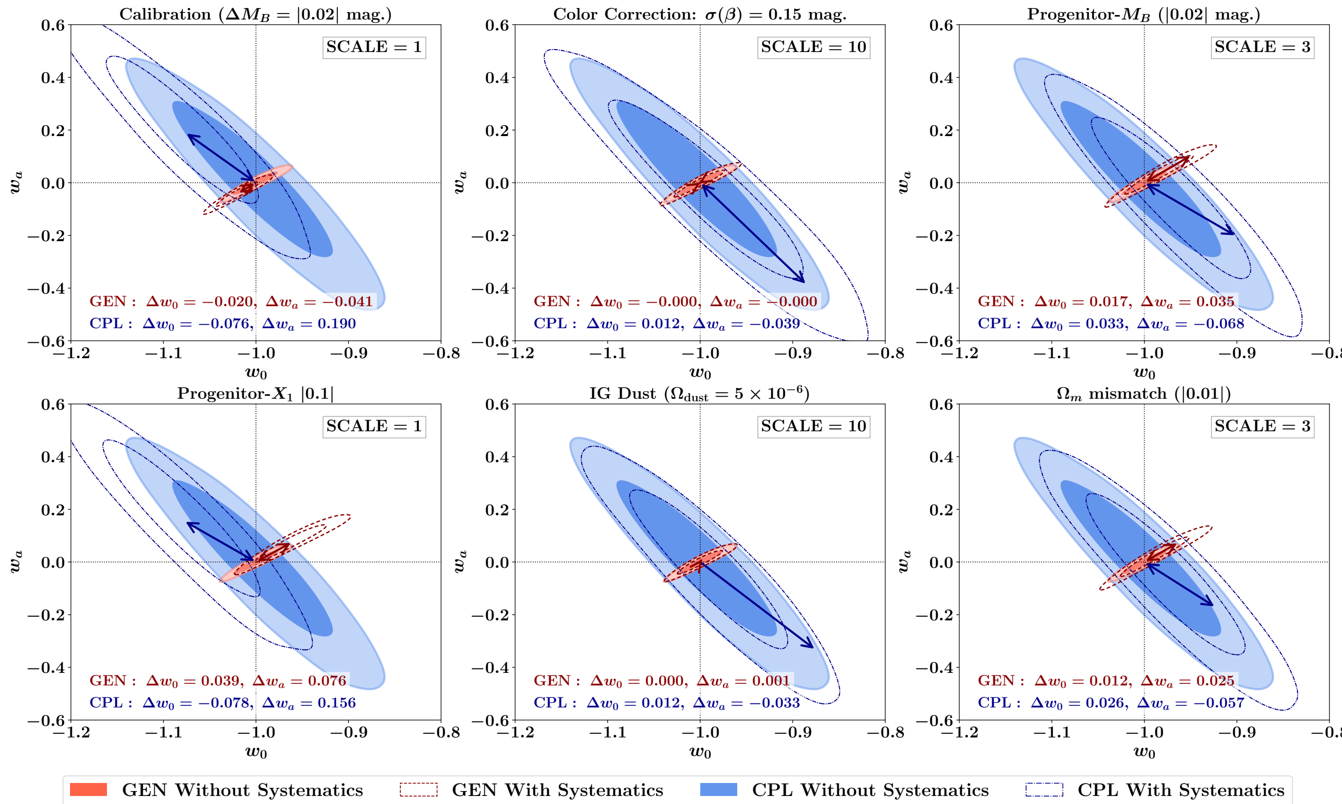

FIG. 4: Impact of injected SNIa systematics on the w_0–w_a constraints for the CPL vs GEN parametrizations. Panels illustrate how individual systematics shift the recovered contours. Filled contours denote fits without systematics; dashed contours show results after systematic injection.

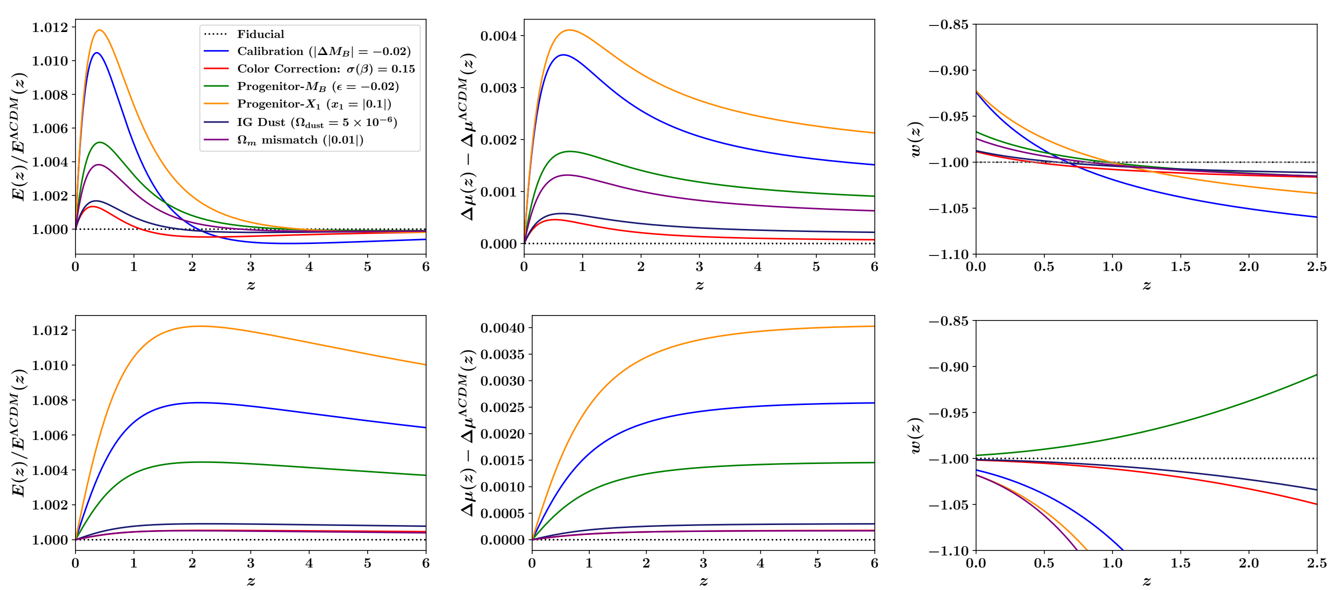

FIG. 5: Effect of systematics injection on the normalised Hubble parameter $E(z)$ (left), distance modulus $\mu(z)$ (middle) and dark energy EoS $w(z)$ (right): Comparison between CPL (top panel) vs GEN (bottom panel) models.

at low redshift, gradually increasing and reaching a maximum around $z \sim 1$, before slowly declining and settling to an approximately constant offset at higher z. For $w(z)$, the behaviour differs qualitatively from the CPL case: the reconstructed EoS tends to remain either entirely in the phantom or non-phantom regime across the redshift range, with systematics primarily shifting its overall amplitude rather than inducing transitions. This pattern underscores that while the CPL model captures a specific range of DE behaviors, the GEN parametrization can accommodate for a broader spectrum, with reconstructed quantities exhibiting distinct and systematic responses to underlying uncertainties.

VII. SUMMARY AND DISCUSSIONS

In this study, we have systematically examined how various instrumental and astrophysical uncertainties in SN-Ia observations can affect dark energy constraints and search for new physics beyond the concordance ΛCDM model. By simulating realistic mock datasets consistent with the Pantheon-Plus SN-Ia sample in addition to DESI-DR2 BAO, and compressed CMB measurements, we quantify the impact of six major sources of systematic bias — photometric calibration, intergalactic dust, progenitor evolution in luminosity and light-curve stretch, color-correction scatter and matter density mismatch in SN-Ia observations — on four time-evolving dark energy parametrizations for equation of state (CPL, JBP, LOG) as well as the parametrization for scale factor (GEN) of the Universe.

Our results show that calibration offsets and progenitor evolution effects dominate the systematic error budget in SN-Ia cosmology. A small magnitude bias ($\Delta M_B \approx 0.02$ mag) can shift the equation of state parameters by $\Delta w_0 \approx -0.1$ and $\Delta w_a \approx +0.5$ in the most flexible models, while progenitor-related evolution in luminosity and stretch induces comparable shifts along the w_0–w_a degeneracy axis. In contrast, intergalactic dust, color correction scatter, and modest density mismatches produce only minor deviations, confirming that their influence remains well below the statistical precision of current SN-Ia datasets.

A key outcome of this work is the identification of a hierarchy in model susceptibility to systematics:

1. JBP exhibits the strongest response to redshift-dependent biases, reflecting its higher-order sensitivity to luminosity evolution.
2. CPL and LOG behave similarly, showing intermediate vulnerability to calibration and progenitor effects.
3. GEN, which parameterizes the expansion rate directly rather than $w(z)$, remains the most robust and stable under all systematic injections. Its minimal response arises from its dependence on a single integral of scale factor $a(t)$, rather than double integrals of $w(z)$, reducing cumulative bias propagation.

These findings highlight that the choice of dark energy parametrization critically shapes the inferred cosmological evolution, particularly when the data are susceptible to unmodelled systematics. Given that the error budgets of Pantheon-Plus and the recent DES-SN-5YR [19] compilation are quite similar, our findings are broadly applicable to both SN-Ia samples, alleviating concerns about dataset-specific deviations. For ongoing and future SN-Ia cosmology programs—such as those conducted by DES, LSST, and Roman—achieving sub-percent calibration precision and accurately modelling population evolution across redshift will be indispensable for robust dark energy inferences.

Finally, the analysis reinforces a central message: apparent signatures of time-varying dark energy may arise from subtle, unaccounted biases in SN-Ia standardization rather than genuine physical departures from ΛCDM and modelling the departure from ΛCDM is crucial in this regard. Mitigating these effects requires coordinated improvements in calibration pipelines, cross-survey photometric harmonization, and empirical modelling of SN progenitor diversity. Future joint analyses incorporating multi-wavelength SN-Ia data, improved host-environment characterization, and cross-validation with BAO and CMB anchors will be key to resolving current expansion-rate anomalies and confirming whether hints of dynamical dark energy persist.

ACKNOWLEDGMENTS

PM acknowledges funding from the Anusandhan National Research Foundation (ANRF), Govt of India, under the National Post-Doctoral Fellowship (File no. PDF/2023/001986). AAS acknowledges the funding from ANRF, Govt of India, under the research grant no. CRG/2023/003984. SD acknowledges support from UK Research and Innovation (UKRI) under the UK government's Horizon Europe funding Guarantee EP/Z000475/1. We acknowledge the use of the HPC facility, Pegasus, at IUCAA, Pune, India. This article/publication is based upon work from COST Action CA21136- "Addressing observational tensions in cosmology with systematics and fundamental physics (CosmoVerse)", supported by COST (European Cooperation in Science and Technology).

[1] N. Aghanim *et al.* (Planck), Astron. Astrophys. **641**, A6 (2020), [Erratum: Astron.Astrophys. 652, C4 (2021)], arXiv:1807.06209 [astro-ph.CO].
[2] M. Tristram *et al.*, Astron. Astrophys. **682**, A37 (2024),

arXiv:2309.10034 [astro-ph.CO].
[3] T. Louis *et al.* (ACT), arXiv preprint (2025), arXiv:2503.14452 [astro-ph.CO].
[4] D. M. Scolnic *et al.* (Pan-STARRS1), Astrophys. J. **859**, 101 (2018), arXiv:1710.00845 [astro-ph.CO].
[5] D. Brout, D. Scolnic, *et al.*, The Astrophysical Journal **938**, 110 (2022).
[6] S. Alam *et al.* (BOSS), Mon. Not. Roy. Astron. Soc. **470**, 2617 (2017), arXiv:1607.03155 [astro-ph.CO].
[7] S. Alam *et al.* (eBOSS), Phys. Rev. D **103**, 083533 (2021), arXiv:2007.08991 [astro-ph.CO].
[8] A. G. Adame *et al.* (DESI), JCAP **09**, 008, arXiv:2411.12021 [astro-ph.CO].
[9] S. Weinberg, Rev. Mod. Phys. **61**, 1 (1989).
[10] P. J. E. Peebles and B. Ratra, Rev. Mod. Phys. **75**, 559 (2003), arXiv:astro-ph/0207347.
[11] T. Padmanabhan, Phys. Rept. **380**, 235 (2003), arXiv:hep-th/0212290.
[12] A. G. Riess *et al.* (Supernova Search Team), Astron. J. **116**, 1009 (1998), arXiv:astro-ph/9805201.
[13] S. Perlmutter *et al.* (Supernova Cosmology Project), Astrophys. J. **517**, 565 (1999), arXiv:astro-ph/9812133.
[14] A. Goobar and B. Leibundgut, Annual Review of Nuclear and Particle Science **61**, 251–279 (2011).
[15] N. Suzuki *et al.*, Astrophys. J. **746**, 85 (2012), arXiv:1105.3470 [astro-ph.CO].
[16] M. Betoule *et al.* (SDSS), Astron. Astrophys. **568**, A22 (2014), arXiv:1401.4064 [astro-ph.CO].
[17] M. Chevallier and D. Polarski, Int. J. Mod. Phys. D **10**, 213 (2001), arXiv:gr-qc/0009008.
[18] E. V. Linder, Phys. Rev. Lett. **90**, 091301 (2003), arXiv:astro-ph/0208512.
[19] T. M. C. Abbott *et al.* (DES), Astrophys. J. Lett. **973**, L14 (2024), arXiv:2401.02929 [astro-ph.CO].
[20] D. Rubin *et al.*, arXiv preprint (2023), arXiv:2311.12098 [astro-ph.CO].
[21] S. Casertano *et al.* (H0DN), arXiv preprint (2025), arXiv:2510.23823 [astro-ph.CO].
[22] L. Perivolaropoulos and F. Skara, New Astron. Rev. **95**, 101659 (2022), arXiv:2105.05208 [astro-ph.CO].
[23] A. G. Riess and L. Breuval, IAU Symp. **376**, 15 (2022), arXiv:2308.10954 [astro-ph.CO].
[24] E. Di Valentino and D. Brout, eds., *The Hubble Constant Tension*, Springer Series in Astrophysics and Cosmology (Springer, 2024).
[25] G. Efstathiou, Phil. Trans. Roy. Soc. Lond. A **383**, 20240022 (2025), arXiv:2406.12106 [astro-ph.CO].
[26] E. Di Valentino *et al.* (CosmoVerse Network), Phys. Dark Univ. **49**, 101965 (2025), arXiv:2504.01669 [astro-ph.CO].
[27] I. Labbe *et al.*, Nature **616**, 266 (2023), arXiv:2207.12446 [astro-ph.GA].
[28] M. Boylan-Kolchin, Nature Astron. **7**, 731 (2023), arXiv:2208.01611 [astro-ph.CO].
[29] M. Abdul Karim *et al.* (DESI), Phys. Rev. D **112**, 083514 (2025), arXiv:2503.14739 [astro-ph.CO].
[30] M. Abdul Karim *et al.* (DESI), Phys. Rev. D **112**, 083515 (2025), arXiv:2503.14738 [astro-ph.CO].
[31] K. Lodha *et al.* (DESI), Phys. Rev. D **112**, 083511 (2025), arXiv:2503.14743 [astro-ph.CO].
[32] G. Gu *et al.* (DESI), Nature Astron. 10.1038/s41550-025-02669-6 (2025), arXiv:2504.06118 [astro-ph.CO].
[33] P. Mukherjee and A. A. Sen, Rept. Prog. Phys. **88**, 098401 (2025), arXiv:2505.19083 [astro-ph.CO].
[34] S. Gupta Choudhury, P. Mukherjee, and A. A. Sen, arXiv preprint (2025), arXiv:2510.09602 [astro-ph.CO].
[35] J. Nordin *et al.*, Astrophys. J. **734**, 42 (2011), arXiv:1012.4430 [astro-ph.CO].
[36] A. G. Riess *et al.*, Astrophys. J. Lett. **934**, L7 (2022), arXiv:2112.04510 [astro-ph.CO].
[37] A. G. Riess *et al.*, Astrophys. J. **977**, 120 (2024), arXiv:2408.11770 [astro-ph.CO].
[38] D. Brout *et al.*, Astrophys. J. **938**, 111 (2022), arXiv:2112.03864 [astro-ph.CO].
[39] M. J. Graham *et al.*, Publ. Astron. Soc. Pac. **131**, 078001 (2019), arXiv:1902.01945 [astro-ph.IM].
[40] S. Dhawan, A. Goobar, M. Smith, J. Johansson, M. Rigault, J. Nordin, *et al.*, Monthly Notices of the Royal Astronomical Society **510**, 2228–2241 (2021).
[41] M. Rigault *et al.*, Astron. Astrophys. **694**, A1 (2025), arXiv:2409.04346 [astro-ph.CO].
[42] S. Dhawan, B. Popovic, and A. Goobar, Mon. Not. Roy. Astron. Soc. **540**, 1626 (2025), arXiv:2409.18668 [astro-ph.CO].
[43] A. Goobar, S. Dhawan, and D. Scolnic, Monthly Notices of the Royal Astronomical Society: Letters **477**, L75–L79 (2018).
[44] S. Dhawan *et al.*, Mon. Not. Roy. Astron. Soc. **535**, 2939 (2024), arXiv:2407.16492 [astro-ph.HE].
[45] M. Ginolin, M. Rigault, M. Smith, Y. Copin, F. Ruppin, *et al.*, Astronomy & Astrophysics **695**, A140 (2025).
[46] B. Popovic, D. Brout, R. Kessler, and D. Scolnic, The Astrophysical Journal **945**, 84 (2023).
[47] A. A. Sen and S. Sethi, Phys. Lett. B **532**, 159 (2002), arXiv:gr-qc/0111082.
[48] U. Mukhopadhyay, S. Haridasu, A. A. Sen, and S. Dhawan, Phys. Rev. D **110**, 123516 (2024), arXiv:2407.10845 [astro-ph.CO].
[49] H. K. Jassal, J. S. Bagla, and T. Padmanabhan, Physical Review D **72**, 10.1103/physrevd.72.103503 (2005).
[50] G. Efstathiou, Monthly Notices of the Royal Astronomical Society **310**, 842–850 (1999).
[51] S. Brieden, H. Gil-Marín, and L. Verde, JCAP **04**, 023, arXiv:2212.04522 [astro-ph.CO].
[52] P. Lemos and A. Lewis, Phys. Rev. D **107**, 103505 (2023), arXiv:2302.12911 [astro-ph.CO].
[53] R. Tripp, Astron. Astrophys. **331**, 815 (1998).
[54] R. Tripp and D. Branch, Astrophys. J. **525**, 209 (1999), arXiv:astro-ph/9904347.
[55] B. Popovic, D. Brout, R. Kessler, D. Scolnic, and L. Lu, The Astrophysical Journal **913**, 49 (2021).
[56] `https://github.com/dfm/emcee.git`.
[57] D. Foreman-Mackey, D. W. Hogg, D. Lang, and J. Goodman, PASP **125**, 306 (2013), 1202.3665.
[58] `https://github.com/cmbant/getdist.git`.
[59] A. Lewis, JCAP **08**, 025, arXiv:1910.13970 [astro-ph.IM].
[60] M. Vincenzi *et al.* (DES), Astrophys. J. **975**, 86 (2024), arXiv:2401.02945 [astro-ph.CO].
[61] R. J. Foley *et al.*, Mon. Not. Roy. Astron. Soc. **475**, 193 (2018), arXiv:1711.02474 [astro-ph.HE].
[62] B. Ménard, R. Scranton, M. Fukugita, and G. Richards, Monthly Notices of the Royal Astronomical Society **405**, 1025 (2010).
[63] J. C. Weingartner and B. T. Draine, The Astrophysical Journal **548**, 296 (2001).
[64] C. Balland, S. Baumont, S. Basa, M. Mouchet, D. A. Howell, P. Astier, *et al.*, Astronomy & Astrophysics **507**, 85–103 (2009).

[65] C. Balland, F. Cellier-Holzem, C. Lidman, *et al.*, Astronomy & Astrophysics **614**, A134 (2018).

[66] R. S. Ellis *et al.* (SNLS), Astrophys. J. **674**, 51 (2008), arXiv:0710.3896 [astro-ph].

[67] K. Maguire, M. Sullivan, R. S. Ellis, P. E. Nugent, D. A. Howell, A. Gal-Yam, *et al.*, Monthly Notices of the Royal Astronomical Society **426**, 2359–2379 (2012).

[68] R. J. Foley, A. V. Filippenko, R. Kessler, B. Bassett, J. A. Frieman, P. M. Garnavich, S. W. Jha, H. Lampeitl, A. G. Riess, M. Sako, D. P. Schneider, J. Sollerman, and M. Smith, The Astronomical Journal **143**, 113 (2012).

[69] M. E. Moreno-Raya, A. R. López-Sánchez, M. Mollá, L. Galbany, J. M. Vílchez, and A. Carnero, Monthly Notices of the Royal Astronomical Society **462**, 1281–1306 (2016).

[70] M. E. Moreno-Raya, M. Mollá, A. R. López-Sánchez, L. Galbany, J. M. Vílchez, A. C. Rosell, and I. Domínguez, The Astrophysical Journal Letters **818**, L19 (2016).

[71] M. J. Childress, C. Wolf, and H. J. Zahid, Monthly Notices of the Royal Astronomical Society **445**, 1898 (2014), https://academic.oup.com/mnras/article-pdf/445/2/1898/18198330/stu1892.pdf.

[72] Nicolas, N., Rigault, M., Copin, Y., Graziani, R., Aldering, G., Briday, M., Kim, Y.-L., Nordin, J., Perlmutter, S., and Smith, M., A & A **649**, A74 (2021).

[73] X. T. Tang, D. Brout, T. Karwal, C. Chang, V. Miranda, and M. Vincenzi, Astrophys. J. Lett. **983**, L27 (2025), arXiv:2412.04430 [astro-ph.CO].